nature physics

ARTICLES

PUBLISHED ONLINE: 28 APRIL 2014 | DOI: 10.1038/NPHYS2940

Universal features in the energetics of symmetry breaking

É. Roldán[1†], I. A. Martínez[2†], J. M. R. Parrondo[1*] and D. Petrov[2,3‡]

A breaking of symmetry involves an abrupt change in the set of microstates a system can explore. This change has unavoidable thermodynamic implications: a shrinkage of the microstate set results in an entropy decrease, which eventually needs to be compensated by heat dissipation and hence requires work. On the other hand, in a spontaneous symmetry breaking, the available phase-space volume changes without the need for work, yielding an apparent entropy decrease. Here we show that this entropy decrease is a key ingredient of a Szilard engine and Landauer's principle, and perform a direct measurement of the entropy change along symmetry-breaking transitions for a Brownian particle subject to a bistable potential realized through two optical traps. The experiment confirms theoretical results based on fluctuation theorems, enables the construction of a Szilard engine extracting energy from a single thermal bath, and shows that a signature of a symmetry breaking in a system's energetics is observable.

When a symmetry is broken, a system 'makes a choice' from among a set of instances $i = 1, \ldots, m$. For a classical infinite system, symmetry breaking (SB) consists of a sudden loss of ergodicity, that is, a change in the set of available states: the whole phase space Γ is partitioned into non-overlapping regions Γ_i, corresponding to the different instances $i = 1, \ldots, m$. The partition occurs when a certain control parameter λ crosses a critical value λ_c above which the system can no longer move spontaneously from one region to another and gets confined within Γ_i with probability p_i, $\sum_i p_i = 1$. The notion of SB can be extended to finite systems with metastable states. The confinement or loss of ergodicity is not strict in this case: the system can jump from a region Γ_i to another Γ_j. However, if the average residence time in each region is much larger than the timescale of the process under consideration, one can talk about an effective SB. In this case, the SB transition is not localized at a single value of the control parameter λ, but is rather a continuous transition where metastable states develop.

The energetics associated with SB transitions and, in general, with the manipulation of metastable states has special relevance to a number of interesting physical situations, some of them realized experimentally in the past few years. The original Szilard engine, a refined version of the original Maxwell demon, can extract work from a single thermal bath using the information created in a SB (refs 1–4). Landauer's principle accounts for the minimum dissipation associated with the erasure of information, which is a manipulation of the two metastable states making up a single-bit memory[1]. The erasure can be interpreted as the restoration of a broken symmetry (see below) and has been reproduced with a Brownian particle in a double-well potential created by optical tweezers[5]. In molecules, metastable states correspond to different molecular conformations as well as to kinetic states of special relevance to biophysics. The energetics of processes involving metastable states has become a tool to measure conformational free energies in those contexts[6–8]. An extended version of the non-equilibrium work theorem relates the probability distribution of the work in a process connecting two metastable states with their conformational free energies. Ref. 6 applied this result to numerical simulations of switches between two different conformations of alanine dipeptide. In refs 7,8, this generalized work theorem is used to estimate, from stretching experiments, the conformational free energy of DNA hairpins that possess intermediate or misfolded kinetic states.

Here, we report on an experimental realization of a SB consisting of a continuous transition from a single-well to a double-well potential affecting a Brownian particle. We reproduce the transition by moving apart two optical traps and then measure the heat dissipated by the particle to the surrounding water that acts as a thermal reservoir. An electrostatic field acting on electrical charges on the particle's surface allows us to tune the bias towards one or the other trap and explore the relation between the energetics of the SB and the probability of adopting one of the instances. We finally build a Szilard engine as a SB followed by the restoration of that symmetry under different conditions. This process completes a cycle that extracts energy from the thermal bath if the electrostatic field along the process is properly chosen.

SB and symmetry restoration

Consider a system with Hamiltonian $\mathcal{H}(x;\lambda)$ ($x \in \Gamma$), depending on a control parameter λ, and an isothermal process at temperature T involving a SB, where the parameter changes in time as $\lambda(t)$ with $t \in [t_{\rm ini}, t_{\rm fin}]$. The average work required to complete the process, when the system adopts instance i, is bound by

$$\langle W \rangle_i^{(\rm SB)} - \Delta F_i \geq kT \ln p_i \qquad (1)$$

where k is the Boltzmann constant and $\Delta F_i = F_{{\rm fin},i} - F_{\rm ini}$ is the change in free energy. The initial free energy is defined as usual, $F_{\rm ini} = -kT \ln Z(T, \lambda(t_{\rm ini}))$, where $Z(T,\lambda) = \int_\Gamma {\rm d}x\, {\rm e}^{-\beta \mathcal{H}(x;\lambda)}$ is the partition function of the system. On the other hand, the final free

[1]Departamento de Física Atómica, Molecular y Nuclear and GISC, Universidad Complutense de Madrid, 28040 Madrid, Spain, [2]ICFO—Institut de Ciències Fotòniques, Mediterranean Technology Park, Av. Carl Friedrich Gauss, 3, 08860 Castelldefels (Barcelona), Spain, [3]ICREA—Institució Catalana de Recerca i Estudis Avançats, Passeig Lluís Companys, 23, 08010 Barcelona, Spain. †These authors contributed equally to this work. ‡Deceased. *e-mail: parrondo@fis.ucm.es

energy $F_{\mathrm{fin},i} = -kT \ln Z_i(T, \lambda(t_{\mathrm{fin}}))$ is a conformational free energy defined in terms of the partition function restricted to the region Γ_i, that is, $Z_i(T,\lambda) = \int_{\Gamma_i} \mathrm{d}x\, \mathrm{e}^{-\beta \mathcal{H}(x;\lambda)}$. The bound in equation (1) is met with equality if the process is quasistatic. Recalling the relation between the free energy, F, the internal energy E, and the entropy S of a system, $F = E - TS$, and the first law of thermodynamics $\Delta E = W + Q$, where Q is the heat or energy transfer from the thermal reservoir to the system, we easily derive a bound for the conformational entropy production:

$$\langle S_{\mathrm{prod}} \rangle_i^{(\mathrm{SB})} \equiv \Delta S_i - \frac{\langle Q \rangle_i^{(\mathrm{SB})}}{T} \geq k \ln p_i \tag{2}$$

A rigorous proof of these bounds follows from fluctuation theorems (Supplementary Section I.A). However, the origin of the term $k \ln p_i$ in equations (1) and (2) can be easily understood. A SB comprises a contraction of the set of available states from Γ to Γ_i without the need for any extra work[2,3]. This amounts to an increase in free energy $-kT \ln(Z_i/Z)$ that is not compensated by work and heat dissipation. Assuming an instantaneous SB, $p_i = Z_i/Z$, yielding the extra term $kT \ln p_i$ in equations (1) and (2).

This work-free shrinkage of the available phase space is entirely due to the SB transition and is not in contradiction with the second law of thermodynamics, because the final state $\rho_i(x)$ is not in complete equilibrium and the final entropy cannot be considered as a true thermodynamic entropy. In some contexts, S_i and F_i are called, respectively, the conformational entropy and the conformational free energy, but they are not true thermodynamic potentials (they are not state functions; see, for example, ref. 9). However, both are useful tools for analysing the energetics of processes involving SB transitions[9–11] and non-equilibrium states[12]. An alternative interpretation of the compatibility between the second law and the decrease of entropy in equation (2) is that the latter is compensated by an increase of the meso- or macroscopic uncertainty, quantified by the Shannon entropy of the SB outcome, $H(p_i) = -\sum_i p_i \ln p_i$. Note that the average of equation (1) over p_i yields precisely $kT\, H(p_i)$. This interpretation can be formulated in a rigorous way using non-equilibrium free energies[11,12] (Supplementary Section I.D).

Similar inequalities hold for a process where a symmetry is restored. To assess the energetics of a symmetry restoration (SR) we have to consider the time reversal of the restoration, which is a SB. Let us call $\tilde{p}_i$ the probability that the system adopts instance i in this SB resulting from the time reversal of the original process. Under time reversal, the reversible work and the increase in the free energy change sign. Therefore (Supplementary Section I.B, for a detailed proof):

$$\langle W \rangle_i^{(\mathrm{SR})} - \Delta F_i \geq -kT \ln \tilde{p}_i \tag{3}$$

where now $\Delta F_i = F_{\mathrm{fin}} - F_{\mathrm{ini},i}$ is the free-energy change of the SR. Note that now it is the initial free energy that depends on the instance i. For the entropy:

$$\langle S_{\mathrm{prod}} \rangle_i^{(\mathrm{SR})} \geq -k \ln \tilde{p}_i \tag{4}$$

The aim of this paper is to check experimentally equations (2) and (4), which have important implications in the thermodynamics of information processing and the foundations of statistical mechanics. For instance, Landauer's principle follows immediately from equation (3) applied to a one-bit memory consisting of a physical system with two stable states, 0 and 1, each one with the same free energy $F_0 = F_1$. The minimal cost of erasing a bit or, more precisely, to drive bit $i = 0$ or 1 to the state 0 (restore-to-zero operation) is $\langle W \rangle_i^{\mathrm{erasure}} \geq -kT \ln \tilde{p}_i + \Delta F_i = -kT \ln \tilde{p}_i$ for $i = 0$ or 1, because in both cases $\Delta F_i = F_0 - F_i = 0$. If the initial bit is unknown, the best we can do is $\tilde{p}_i = 1/2$ and $\langle W \rangle_i^{\mathrm{erasure}} \geq kT \ln 2$ (refs 1,5,12).

The energetics of the Szilard engine[10,13,14] can also be easily reproduced from equations (1) and (3). In the Szilard set-up, a system undergoes a SB and chooses between two instances 0 or 1 with probability p_0 and p_1, respectively. Then we measure the instance that has been chosen and restore the broken symmetry driving the system back to the original state through some protocol $\lambda_i(t)$. The time reversal of this protocol is a SB transition with possibly different probabilities $\tilde{p}_j^i$. Note that the superscript i refers to the protocol $\lambda_i(t)$ implemented when i is measured, whereas the subscript j refers to the probability of obtaining outcome j if the protocol $\lambda_i(t)$ is reversed[9,14]. The work necessary to implement the SB is bound by equation (1) and the work necessary to restore the symmetry is bound by equation (3). Therefore, the total average work that we have to perform to run the whole cycle obeys

$$\begin{aligned} \langle W \rangle &= \sum_i p_i \left[\langle W \rangle_i^{(\mathrm{SB})} + \langle W \rangle_i^{(\mathrm{SR})} \right] \\ &\geq kT \sum_i p_i \ln \frac{p_i}{\tilde{p}_i^i}, \end{aligned} \tag{5}$$

and $\langle S_{\mathrm{prod}} \rangle = \langle W \rangle / T$. In the case of the original Szilard engine, $p_i = 1/2$ and $\tilde{p}_i^i = 1$, yielding $\langle W \rangle \geq -kT \ln 2$, that is, the extraction of an energy $kT \ln 2$ in a cycle. If the demon does not use information from the measurement performing always the same protocol, that is, $\lambda_i(t) = \lambda(t)$, then $\tilde{p}_j^i = \tilde{p}_j$ is normalized to unity $\sum_i \tilde{p}_i = 1$ yielding $\langle W \rangle = kTD(p_i || \tilde{p}_i) \geq 0$, where $D(p||q)$ is the relative entropy between the two probability distributions p and q (refs 9,15). To build a Szilard engine, it is enough to find p_i and $\tilde{p}_i^i$ such that the average work $\langle W \rangle$ in equation (5) is negative; for instance by choosing protocols where $\tilde{p}_i^i > p_i$ (see below for an explicit construction of the engine and Supplementary Section I.C, for an illustration of equation (5)).

Experimental test

Inequalities (2) and (4) are universal. They do not depend on the details of the SB or even on the physical nature of the system under consideration, as far as the SB is carried out at temperature T, that is, in contact with a thermal reservoir that induces canonical equilibrium distributions in the system. It is worth noting that in small isolated systems, characterized by microcanonical equilibrium distributions, phase transitions[16] and the trade-off between information and entropy in Maxwell demons[3,17] exhibit interesting peculiarities. Here, we test inequalities (2) and (4) experimentally using a Brownian particle in an optical trapping potential with a time-dependent profile. The particle is surrounded by water at room temperature and its equilibrium distribution is well described by a canonical ensemble. We study the motion of a polystyrene spherical bead (1 μm diameter) suspended in water in the presence of two optical traps (Methods). One of the traps, labelled F, is held fixed at $x = 0$ (Fig. 1, top panel). The other trap, labelled M, is moved along the x axis following the four-step protocol depicted in the top panel in Fig. 1. Initially the two traps with their centres separated by a distance $L_{\mathrm{ini}} = 910$ nm are at rest for a period of time $\tau_1 = 0.5$ s (step 1). Then trap M is moved along the x axis at constant velocity v_{trap} for a time τ_2 (step 2). During step 3, the two traps with their centres separated by $L_{\mathrm{fin}} = 1{,}110$ nm are again kept fixed for $\tau_3 = 0.5$ s. Finally, trap M is moved back from L_{fin} to its initial position L_{ini} with velocity $-v_{\mathrm{trap}}$ for a time $\tau_4 = \tau_2$ (step 4). The total duration of the cycle is $\tau = \sum_{i=1}^{4} \tau_i = 2\tau_2 + 1$ s. By cyclically repeating this protocol, we can study both the SB (steps 1–2–3) and the SR (steps 3–4–1).

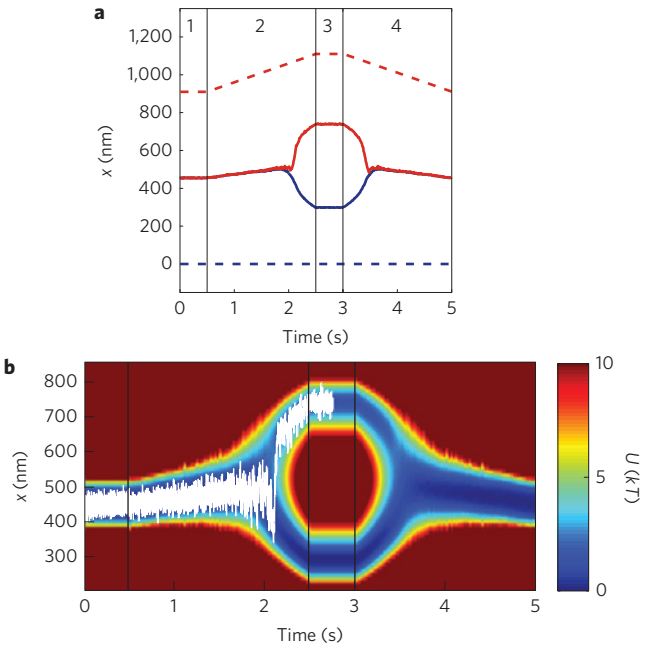

Figure 1 | Experimental protocol of symmetry breaking and symmetry restoration. a, Positions of the fixed (F) trap (blue dashed line) and moving (M) trap (red dashed line) as functions of time during the protocol. Ensemble average position of the trapped bead after implementing the protocol cyclically for $t=2{,}400$ s over F trajectories (blue solid line) and M trajectories (red solid line). **b**, Spatial–temporal mapping of the potential $U(x,t)$ obtained from the statistics of trajectories of the bead for $t=2{,}400$ s in the presence of an external force such that $p_F=0.8$. The colour bar on the right indicates the depth of the potential energy (in units of kT). A single trajectory of the bead when it chooses the M trap is also plotted (white line).

Owing to the presence of inherited electrical charges at the surface of the bead, we can bias the motion of the bead towards the M or F trap by applying a voltage to electrodes inserted in the fluid chamber[18] (Supplementary Section II).

The protocol can be considered quasistatic for velocities around 100 nm s^{-1} or lower, for which the heat dissipation due to friction force is of the order of $\gamma v_{\rm trap}^2 \approx 10^{-22}$ J s^{-1} $\approx 0.02\,kT$ s^{-1}, where $\gamma=6\pi R\eta$ is the friction coefficient, $R=0.5\,\mu$m is the radius of the bead, and $\eta=8.9\times10^{-4}$ Pa s is the dynamic viscosity of water at 25 °C. We have implemented two quasistatic protocols with $v_{\rm trap}=100$ nm s^{-1}, $\tau_2=2$ s, and $v_{\rm trap}=36.36$ nm s^{-1}, $\tau_2=5.5$ s.

During step 2, Kramers transitions[19] trigger the SB. This can be seen clearly in the trajectory of the bead presented in the bottom panel of Fig. 1. At the end of the SB protocol (steps 1–2–3), Kramers transitions are not observable, and one can unambiguously distinguish two final meso-states for the bead position: the particle either stays at the F trap (F trajectories) or moves with the M trap (M trajectories). In the top panel of Fig. 1, we show the ensemble averages of the position of the bead calculated over F (blue curve) and M (red curve) trajectories.

The potential $U(x,t)$ along the protocol (bottom panel in Fig. 1) was obtained from the empirical probability density function (PDF) calculated combining data from both the SB and the SR. In the SB, the potential changes smoothly from monostable to bistable, with an energy barrier that increases with time. The Kramers first-passage time from the F to the M trap, $\tau_K^{\rm F\to M}$, calculated from the potential shown in Fig. 1 and assuming one-dimensional motion, increases with time smoothly from $\tau_{\rm min}=0$ s to $\tau_{\rm max}=5.7\times10^5$ s $=6.62$ days. For the two quasistatic protocols, the total duration of the process is of the order of seconds. Consequently, ergodicity is effectively broken because the particle does not have enough time to jump from the F to the M trap at the end of the process (Supplementary Section V).

From the energy landscape $U(x,t)$, we were able to measure the heat or energy transfer from the thermal reservoir to the Brownian particle for individual trajectories[20,21] and for different values of the external force and therefore of the probability of choice p_i (Methods and Supplementary Section III). The average conformational entropy production over the M and F realizations for the SB and SR is calculated from the heat and the Shannon entropy, using equation (2), and plotted in Fig. 2 as a function of $\ln p_i$ for the SB (Fig. 2a) and $\ln \tilde{p}_i$ for the SR (Fig. 2b). These figures are the main result of the paper. The experiment confirms the dependence of the entropy on the probability of adopting a given instance given by equation (2). In the case of the SB, the negative conformational entropy production is clearly observed and the theoretical dependence is reproduced, except for very low probabilities $p_i \lesssim e^{-2} \simeq 0.05$. We have included error bars calculated using the statistical dispersion of the heat over a large number of cycles. The error in the empirical potential $U(x,t)$ and in the Shannon entropy of the initial and final states, however, has not been taken into account and could be significant for small p_i, because the number of data points is low. This lack of statistics could explain the discrepancy between the experimental result and

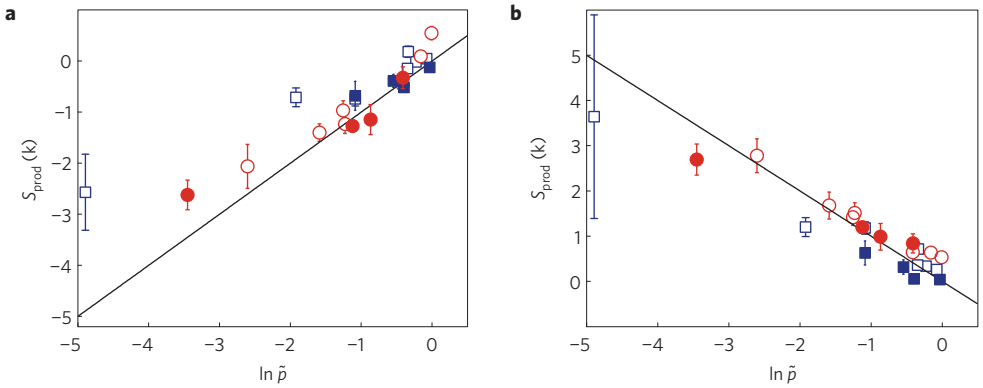

Figure 2 | Energetics of symmetry breaking and symmetry restoration. a, Ensemble average conformational entropy production in the symmetry breaking (SB), $\langle S_{\rm prod}\rangle_i^{\rm (SB)}$ (in units of k) as a function of the probability p_i of adopting instance $i=$ fixed (F), moving (M). **b**, Ensemble average conformational entropy production in the symmetry restoration (SR), $\langle S_{\rm prod}\rangle_i^{\rm (SR)}$ (in units of k) as a function of $\tilde{p}_i$. Results shown as open symbols were obtained using the fast protocol ($\tau_2=2$ s), and results shown as filled symbols were obtained using the slow protocol ($\tau_2=5.5$ s). Blue squares represent the ensemble averages over F trajectories, and red circles represent the averages over M trajectories. Error bars were obtained using a statistical significance of 90%.

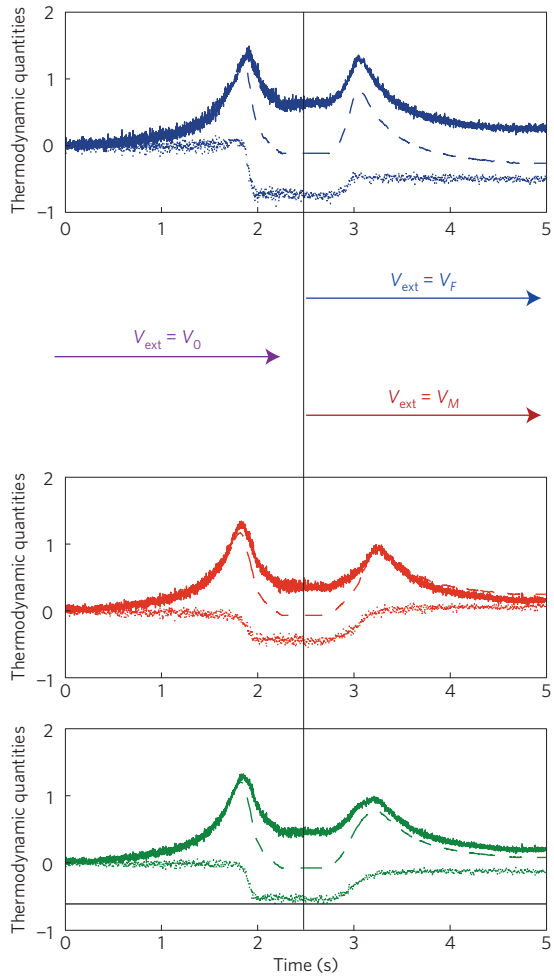

Figure 3 | Experimental realization of the Szilard engine. The average heat (solid lines, in units of kT), the Shannon entropy of the trajectory distribution (dashed lines, in units of k) and the average entropy production (dotted lines, in units of k) as functions of time. The upper plot (blue curves) corresponds to averages over trajectories that end in the fixed (F) trap, the middle plot (red curves) to averages over trajectories that end in the moving (M) trap, and the lower plot shows averages over all trajectories (green curves). The feedback protocol is indicated by the arrows. The vertical black line separates the symmetry breaking and the symmetry restoration processes. The symmetry breaking is created with an external voltage $V_{ext} = V_0$ that induces probabilities $p_F = 0.35$, $p_M = 0.65$. When the particle chooses the fixed trap (blue) the symmetry is restored changing the voltage to $V_{ext} = V_F$, and so biasing the potential towards the fixed trap ($\tilde{p}_F = 0.93$). When the particle ends in the moving trap (red), the symmetry is restored at a voltage $V_{ext} = V_M$, biasing the potential towards the moving trap ($\tilde{p}_M = 0.99$). We also indicate in the bottom figure the value of the relative entropy $D(p_i||\tilde{p}_i) = \sum_i p_i \ln(p_i/\tilde{p}_i)$ (horizontal black line, lower plot).

the theoretical prediction. The results corresponding to the slow (filled symbols) and the fast (open symbols) protocol are almost indistinguishable, confirming that the quasistatic limit is indeed achieved for the velocities used in the experiment. In Supplementary Section IV, we have also included numerical simulations of the SB for non-quasistatic processes, to characterize how the dissipative work approaches $kT \ln p_i$ in (1), when the total duration τ of the process increases.

Building a Szilard engine

As an illustration of the implications of the previous results, we construct a Szilard engine that extracts energy from a single thermal reservoir, combining the protocols described above. The engine can be implemented with an adequate combination of SB and SR processes where the lower bound for the minimal work in equation (5) is negative. The minimum is attained for $p_i = 1/2$ and $\tilde{p}_i^i = 1$, $i = \mathrm{F}, \mathrm{M}$, as in the original Szilard cycle, but negative work can be achieved for different values of p_i and $\tilde{p}_i^i$. We have performed multiple experiments at different conditions and in three experiments we could achieve a combination of probabilities that gave us a negative average work: $p_\mathrm{F} = 0.35$, $p_\mathrm{M} = 0.65$; $\tilde{p}_\mathrm{M} = 0.99$; and $\tilde{p}_\mathrm{F} = 0.93$. Then, our Szilard engine consists of the following feedback protocol. We start with the external voltage V_0 that gave us the first combination ($p_\mathrm{F} = 0.35$, $p_\mathrm{M} = 0.65$) and measure the bead position after the SB. If the bead is in the fixed trap (blue curves in Fig. 3) we change the external field to the value V_F corresponding to $\tilde{p}_F = 0.93$ and continue the protocol at this value of voltage until the SR is completed. If after the SB the bead is in the moving trap (red curves in Fig. 3), we change the external field to the value V_M that gave us $\tilde{p}_\mathrm{M} = 0.99$ and continue the protocol at this value of voltage until the SR is completed. Finally, the cycle is to be completed by quasistatically tuning the external voltage back to its initial value V_0. This last step has not been implemented in the experiment, but in principle it can be realized with arbitrarily small entropy production. The actual value of the voltages is sensitive to many factors: the construction of the fluid chamber, the optical adjustment of the system, the size of the focal spot of the trap, the chemical composition of the sphere, the output parameters of the generator, and so on. For the specific chamber and set-up of our experiment, the values were $V_0 = 2$ V, $V_\mathrm{M} = 4$ V and $V_\mathrm{F} = 0$ V.

Figure 3 shows the average heat (solid curves), the change in Shannon entropy of the probability distribution of the bead position (dashed curves), and the average entropy production (dotted curves) along the feedback cycle. The averages are taken over trajectories that end in the F trap (upper plot; blue curves), the M trap (middle plot; red curves), and over all trajectories (lower plot; green curves). Note that the average of the thermodynamic parameters over all trajectories is taken using the probabilities in the SB, that is, $\langle S_\mathrm{prod}\rangle^{(\mathrm{SB})} = \sum_i p_i \langle S_\mathrm{prod}\rangle_i^{(\mathrm{SB})}$ for the SB and $\langle S_\mathrm{prod}\rangle^{(\mathrm{SR})} = \sum_i p_i \langle S_\mathrm{prod}\rangle_i^{(\mathrm{SR})}$ for the SR. The entropy produced in the whole cycle, averaged over all trajectories, $\langle S_\mathrm{prod}\rangle = \langle S_\mathrm{prod}\rangle^{(\mathrm{SB})} + \langle S_\mathrm{prod}\rangle^{(\mathrm{SR})}$, is negative, as shown in the lower plot in Fig. 3. Note that despite being negative, the average entropy production along the cycle is greater than $k D(p_i||\tilde{p}_i) = k \sum_i p_i \ln(p_i/\tilde{p}_i)$ (and greater than the minimum entropy that can be produced $\langle S_\mathrm{prod}\rangle/k > D(p_i||\tilde{p}_i) > -H(p_i)$ (refs 10, 13,14)), as predicted by equation (5).

Conclusions

Our experiments show that the signature of a SB in the energetics of a quasistatic process is observable. This signature is relevant in two situations: estimating the free energy of kinetic or metastable states in macromolecules, and the thermodynamics of computation and information processing. In the first case, the energetics can be used to detect the coexistence of otherwise hidden metastable states, and to identify factors that bias the SB towards a given metastable state. In the second case, the dependence of the entropy production on the probability of adopting a given instance at the SB is able to explain in simple terms the energetics of erasure (Landauer's principle) and feedback (Szilard engine). SB is in fact implicit in other models of information motors based on memories with metastable states[22] or separation of time scales[11].

Moreover, this signature is universal: it does not depend on the nature of the physical system or the mechanism inducing the SB. It is rather small for SBs involving a limited number of metastable states. However, it could have implications in the way we assess the entropy of systems which have undergone a SB with a large number of instances (or a continuous SB). For instance, biological evolution can be considered as a succession of SBs, where specific sequences

of DNA were selected over a gigantic number of possibilities. The same can be said about nucleogenesis in the early Universe and other fundamental processes. The conformational entropy in both cases could have experienced a significant decrease, as indicated by equation (2), whose consequences have not yet been explored.

Methods

Experimental set-up. Polystyrene microspheres of diameter 1 μm (G. Kisker-Products for Biotechnology) were diluted in distilled deionized water to a final concentration of a few spheres per millilitre. The spheres were inserted into a custom-made electrophoretic fluid chamber with two electrodes connected to a computer-controlled electric generator and an amplifier. A 1,060 nm optical beam is deflected by an acousto-optical deflector (ISOMET LS55 NIR), expanded and inserted through an oil-immersed objective O1 (Nikon, CFI PL FL 100X NA 1.30) into the fluid chamber. An additional 532 nm optical beam from a laser coupled to a single-mode fibre (OZOptics) is collimated by a (×10, NA = 0.10) microscope objective and passed through the trapping objective. The forward-scattered detection beam is collected by a (×10, NA = 0.10) microscope objective O2, and its back focal-plane field distribution is analysed by a quadrant position detector (New Focus 2911) at an acquisition rate of 1 kHz. The calibrations of the experimental set-up are described in Supplementary Section II.

The individual traps (the fixed trap F and the moving trap M) are generated with a single beam following a time-sharing protocol for the acousto-optical deflector. The alternation of trap positions is controlled by timing signals generated by a modulation generator adjusted to give a high-frequency (20 kHz) square wave with a controllable duty ratio. The time-sharing protocol permitted controlling the position and velocity of the M trap.

The cycle shown in Fig. 1 containing a SB and a SR was repeated with the same bead and electrostatic field for at least 2,400 s, corresponding to 480 cycles for the fast and 200 cycles for the slow protocol.

Data analysis. We inferred the potential generated by the traps and the external field as a function of time, $U(x,t)$, from the bead position histograms. The only data used in the analysis comes from the trajectory of the bead along a number of cycles. As our protocol is quasistatic, we can use as an estimate of the equilibrium probability $\rho_{\rm eq}(x,\lambda(t))$ the empirical PDF of the position of the bead at time t. To improve the statistics and also as an extra check of the consistency of this estimate, we combine data from the SB and the SR processes corresponding to the same value of the external parameter λ. More precisely, we estimate $\rho_{\rm eq}(x,\lambda(t))$ as the PDF of the trajectories of the bead inside two time windows $[t-S/2,t+S/2]$ and $[\tau-t-S/2,\tau-t+S/2]$, of width $S=25$ ms and centred at times t and $\tau-t$, respectively, when both traps are at the same position in steps 2 and 4 of the protocol (Fig. 1). During steps 1 and 3, the potential is constant and therefore we can use data from the whole duration of those steps. The bin size used for the PDFs is $\Delta x=10$ nm. Using these empirical PDFs we can estimate $\hat{U}(x,t)=U(x,t)-kT\ln Z(\lambda(t))=U(x,t)+F(\lambda(t))$ as $-kT\ln\rho_{\rm eq}(x,\lambda(t))$. Note that the heat dissipated to the thermal bath depends only on local properties of the potential. Consequently, the free energy $F(\lambda(t))$ does not enter into the calculation of the production of conformational entropy. We fit our estimate of the potential to a quartic polynomial $\hat{U}(x,t)=a_0(t)+a_1(t)x+a_2(t)x^2+a_3(t)x^3+a_4(t)x^4$—where $a_i(t)$ are time-dependent parameters—using a nonlinear least-squares weighted fit every $\Delta t=1$ ms. The data were weighted by $w(x,t)=\mathrm{e}^{-U(x,t)/kT}$; that is, we favoured the data near the bottom of the wells. The data points that exceed the global minimum of the potential by more than $10kT$ were not considered.

The conformational entropy production associated with a single stochastic trajectory in the SB has two contributions: the change in the entropy of the particle ΔS and the entropy flow to the thermal reservoir $-Q/T$:

$$S_{{\rm prod},i}=\Delta S_i-Q/T$$

The change in conformational entropy of the particle is $\Delta S_i=S_{{\rm fin},i}-S_{\rm ini}$. The initial entropy of the system is given by $S_{\rm ini}=-k\int_\Gamma {\rm d}x\,\rho_{\rm eq}(x,\lambda(t_{\rm ini}))\ln\rho_{\rm eq}(x,\lambda(t_{\rm ini}))$, where the integration is carried out over the whole phase space. On the other hand, at the end of the process the conformational system entropy depends on the path taken by the bead, $S_{{\rm fin},i}=-k\int_{\Gamma_i}{\rm d}x\,\rho_{{\rm eq},i}(x,\lambda(t_{\rm fin}))\ln\rho_{{\rm eq},i}(x,\lambda(t_{\rm fin}))$, where Γ_i $(i=M,F)$ is the phase space accessible to the bead after the SB, depending on the path. To obtain ΔS_i from the experimental trajectories, we use the empirical PDF of the position of the bead using data from the intervals $[0,\tau_1]$ for $\rho_{\rm eq}(x,\lambda(t_{\rm ini}))$ and $[\tau_1+\tau_2,\tau_1+\tau_2+\tau_3]$ for $\rho_{{\rm eq},i}(x,\lambda(t_{\rm fin}))$. To estimate the dissipated heat Q, we use a modified version of stochastic thermodynamics[20,21,23], suitable for potentials that change by small discrete steps (Supplementary Section III).

Received 21 October 2013; accepted 6 March 2014; published online 28 April 2014

References

1. Leff, H. S. & Rex, A. F. *Maxwell's Demon. Entropy, Information, Computing* (Adam Hilger, 1990).
2. Parrondo, J. M. R. The Szilard engine revisited: Entropy, macroscopic randomness, and symmetry breaking phase transitions. *Chaos* **11,** 725–733 (2001).
3. Marathe, R. & Parrondo, J. M. R. Cooling classical particles with a microcanonical Szilard engine. *Phys. Rev. Lett.* **104,** 245704 (2010).
4. Toyabe, S., Sagawa, T., Ueda, M., Muneyuki, E. & Sano, M. Experimental demonstration of information-to-energy conversion and validation of the generalized Jarzynski equality. *Nature Phys.* **6,** 988–992 (2010).
5. Bérut, A. *et al.* Experimental verification of Landauer's principle linking information and thermodynamics. *Nature* **483,** 187–189 (2012).
6. Maragakis, P., Spichty, M. & Karplus, M. A differential fluctuation theorem. *J. Phys. Chem. B* **112,** 6168–6174 (2008).
7. Junier, I., Mossa, A., Manosas, M. & Ritort, F. Recovery of free energy branches in single molecule experiments. *Phys. Rev. Lett.* **102,** 070602 (2009).
8. Alemany, A., Mossa, A., Junier, I. & Ritort, F. Experimental free-energy measurements of kinetic molecular states using fluctuation theorems. *Nature Phys.* **8,** 688–694 (2012).
9. Horowitz, J. M. & Parrondo, J. M. R. Optimizing non-ergodic feedback engines. *Acta. Phys. Pol. B* **44,** 803–814 (2013).
10. Sagawa, T. & Ueda, M. Minimal energy cost for thermodynamic information processing: Measurement and information erasure. *Phys. Rev. Lett.* **102,** 250602 (2009).
11. Horowitz, J. M., Sagawa, T. & Parrondo, J. M. R. Imitating chemical motors with optimal information motors. *Phys. Rev. Lett.* **111,** 010602 (2013).
12. Esposito, M. & Van den Broeck, C. Second law and Landauer principle far from equilibrium. *Europhys. Lett.* **95,** 40004 (2011).
13. Horowitz, J. M. & Vaikuntanathan, S. Nonequilibrium detailed fluctuation theorem for repeated discrete feedback. *Phys. Rev. E* **82,** 061120 (2010).
14. Horowitz, J. M. & Parrondo, J. M. R. Designing optimal discrete-feedback thermodynamic engines. *New J. Phys.* **13,** 123019 (2011).
15. Kawai, R., Parrondo, J. M. R. & den Broeck, C. V. Dissipation: The phase-space perspective. *Phys. Rev. Lett.* **98,** 080602 (2007).
16. Dunkel, J. & Hilbert, S. Phase transitions in small systems: Microcanonical vs. canonical ensembles. *Physica A* **370,** 390–406 (2006).
17. Vaikuntanathan, S. & Jarzynski, C. Modeling Maxwell's demon with a microcanonical Szilard engine. *Phys. Rev. E* **83,** 061120 (2011).
18. Martinez, I. A., Roldán, E., Parrondo, J. M. R. & Petrov, D. Effective heating to several thousand kelvin of an optically trapped sphere in a liquid. *Phys. Rev. E* **87,** 032159 (2013).
19. Hänggi, P., Talkner, P. & Borkovec, M. Reaction-rate theory: fifty years after Kramers. *Rev. Mod. Phys.* **62,** 251–342 (1990).
20. Sekimoto, K. Langevin equation and thermodynamics. *Prog. Theor. Phys. Suppl.* **130,** 17–27 (1998).
21. Seifert, U. Stochastic thermodynamics, fluctuation theorems and molecular machines. *Rep. Prog. Phys.* **75,** 126001 (2012).
22. Mandal, D. & Jarzynski, C. Work and information processing in a solvable model of Maxwell's demon. *Proc. Natl Acad. Sci. USA* **109,** 11641–11645 (2012).
23. Blickle, V. & Bechinger, C. Realization of a micrometre-sized stochastic heat engine. *Nature Phys.* **8,** 143–146 (2011).

Acknowledgements

I.A.M. and D.P. acknowledge financial support from the Fundació Privada Cellex Barcelona, Generalitat de Catalunya grant 2009-SGR-159, and from the Spanish Ministry of Science and Innovation (MICINN FIS2008-00114, FIS2011-24409). E.R. and J.M.R.P. acknowledge fruitful discussions with S. Grill, M. Jahnel, M. Behrndt, J. M. Horowitz and L. Dinís, and financial support from grants ENFASIS (Spanish Government) and MODELICO (Comunidad de Madrid). This article is dedicated to the memory of D. Petrov, leader of the Optical Tweezers group at ICFO, who passed away on 3 February 2014.

Author contributions

E.R. analysed experimental data, supported theoretical aspects and the design of the experiment, and performed computer simulations. I.A.M. designed the experiment, and obtained all experimental data. J.M.R.P. proposed and established the project, and developed its theoretical aspects. D.P. designed and supervised the experiment. All authors wrote the manuscript.

Additional information

Supplementary information is available in the online version of the paper. Reprints and permissions information is available online at www.nature.com/reprints. Correspondence and requests for materials should be addressed to J.M.R.P.

Competing financial interests

The authors declare no competing financial interests.